

Effects of n-type doping in InAs/GaAs quantum dot layer on current-voltage characteristic of intermediate band solar cells

Yong-Xian Gu,¹ Xiao-Guang Yang,¹ Hai-Ming Ji,¹ Peng-Fei Xu,¹ and Tao Yang^{1, a)}

*Key Laboratory of Semiconductor Materials, Institute of Semiconductors,
Chinese Academy of Sciences, P.O. Box 912, Beijing 100083,
China*

We investigated the current-voltage characteristic of InAs/GaAs quantum dot intermediate band solar cells (QD IBSCs) with different n-type doping density in the QD layer. The n-type doping evidently increases the open circuit voltage, meanwhile decreases the short circuit current density, and leads to the conversion efficiency approaching that of the control solar cell, that is the major role of n-type doping is to suppress the effects of QDs on the current-voltage characteristic. Our model adopts practical parameters for simulation rather than those from detailed balanced method, so that the results in our simulation are not overestimated.

^{a)}Electronic mail: tyang@semi.ac.cn

I. INTRODUCTION

Intermediate band solar cells (IBSCs) are expected to be the third generation photovoltaic devices because of the potential for high energy conversion efficiency.¹⁻³ In addition to the absorption between the conduction band (CB) and the valence band (VB) the same as single junction solar cells, there are transitions from the VB to the IB and from the IB to the CB, it is expected that the IBSCs have the advantages of large increase of short circuit current density, small decrease of open circuit voltage, and enhanced conversion efficiency.

Quantum dots (QDs) are proposed to form the IB,⁴⁻⁷ and another implementation is employing alloys with intrinsic IB.^{8,9} By now the experiments show that the efficiency of InAs/GaAs QD IBSCs are lower than control GaAs solar cells without QDs due to the reduction of open circuit voltage and small increase of short circuit current density.^{6,7,10}

N-type doping in the i-region are raised to half-fill the IB so that the IB can provide strong absorption in transitions from the IB to both the VB and the CB.¹¹ Modulated δ -doping is generally carried out with sheet density equal to the QD density,¹²⁻¹⁴ the doped layer is a certain distance away from the QD layer, and there is approximately one electron on the dot level per quantum dot because there are two states with different spin. Recently direct doping Si into QDs not only can half-fill the IB but also lead to enhancement of the photoluminescence intensity by a dedicated design doping in the QD's assembling stage,¹⁵ then this method is applied to the IBSC and increase in photocurrent is observed.¹⁶

In this paper, we employ the drift-diffusion model to investigate the effects of InAs/GaAs QDs on current-voltage characteristic in IBSCs by changing n-type doping density in the QD layer. The main difference between this modeling and previous work done on IBSCs, is that previously the current-voltage characteristics are mostly based on the detailed balanced method,^{1,3,17,18} material parameters such as the absorption coefficients, carrier mobilities, etc. are not involved. Although some works adopt drift-diffusion model for the simulation of the device structure, the generation and recombination via the IB are still deduced from the detailed balanced method,^{14,19} because of the large difference between the theoretical and experimental results, it is necessary to adopt practical parameters.

II. THE THEORY MODEL

A. Drift-diffusion model

In solar cells, the electron and hole current equations include both drift and diffusion components,

$$J_n = en\mu_n \frac{d\psi}{dx} - eD_n \frac{dn}{dx}, \quad (1)$$

$$J_p = -ep\mu_p \frac{d\psi}{dx} - eD_p \frac{dp}{dx}, \quad (2)$$

where e is the electron charge, n and p are the electron and hole concentration, μ_n and μ_p are the carrier mobilities, which decrease to small values as doping density increases, D_n and D_p are the carrier diffusion constants determined by the Einstein relation, $D_n = \frac{kT}{e}u_n$ and $D_p = \frac{kT}{e}u_p$.

Drift-diffusion model includes Poisson equation, electron and hole current continuity equations,^{19–21} when considering the role of QDs, the three equations can be written as

$$-\frac{d}{dx} \left(\varepsilon \frac{d\psi}{dx} \right) = e [p - n - fN_I + N_D^+ - N_A^-], \quad (3)$$

$$\frac{dJ_n}{dx} = e(G_{CV} + G_I - R_{CV} - R_{SRH}), \quad (4)$$

$$\frac{dJ_p}{dx} = e(G_{CV} + G_I - R_{CV} - R_{SRH}), \quad (5)$$

where ε is the permittivity of the medium, ψ is the electrostatic potential, N_I is the number of the IB states per unit volume, f is the electron occupation factor in the IB, which will be studied later, N_D^+ is the ionized donors and N_A^- is the ionized acceptors.

$G_{CV} = \int \alpha(\lambda) I_0(\lambda) R(\lambda) \exp[-\alpha(\lambda)x] d\lambda$, is the generation rate of carriers from the VB to CB, where $I_0(\lambda)$ is the intensity of the light at $x = 0$, $\alpha(\lambda)$ is the absorption coefficient of the host material, and $R(\lambda)$ is the reflectivity of the front surface.

G_I is the generation rate of electron hole pairs through absorption of the IB, which will be studied later. $R_{CV} = r_{CV} (np - n_i^2)$ is the direct recombination between the CB and the VB, and r_{CV} is the recombination coefficient.

R_{SRH} is the Shockley-Read-Hall (SRH) recombination between conduction and valance bands,

$$R_{SRH} = \frac{(np - n_i^2)}{\tau_n(p + p_1) + \tau_p(n + n_1)}, \quad (6)$$

where τ_n and τ_p are electron and hole lifetime respectively, $n_1 = n_i \exp\left(\frac{E_t - E_i}{kT}\right)$ and $p_1 = n_i \exp\left(\frac{E_i - E_t}{kT}\right)$, n_i is the intrinsic carrier concentration of the host material, E_t is the defect energy position, which for simplicity is set in the middle of GaAs bandgap, E_i is the intrinsic Fermi energy, k is the Boltzmann constant and T is the temperature of the solar cell.

B. Electron occupation factor and net generation

In most literatures, carrier generation and recombination via the IB are analyzed based on detailed balanced method, finally the results are often overestimated and deviate from experimental results. By adding the light generation components to the derivation process of SRH recombination in textbook,²² the involved four processes for the generation and recombination can be written as:²⁰ The carrier recombination from the CB to the IB

$$R_{CI} = r_{CI}N_I(1 - f)n, \quad (7)$$

the generation from the IB to the CB

$$G_{CI} = e_e N_I f + g_{CI} N_I f, \quad (8)$$

the recombination from the IB to the VB

$$R_{VI} = r_{VI}N_I f p, \quad (9)$$

and the generation from the VB to the IB

$$G_{VI} = e_h N_I(1 - f) + g_{VI} N_I(1 - f), \quad (10)$$

where r_{CI} and r_{VI} are the recombination coefficients, e_e and e_h are the emitting coefficients due to factors such as thermal excitation, g_{CI} and g_{VI} are light generation coefficients proportional to the light intensity and absorption coefficient via the IB.

If there are no optical and electrical injection, the device is in equilibrium with a uniform Fermi level E_{f0} , electron density n_0 in the CB, hole density p_0 in the VB and electron occupation f_0 in the IB, and recombination is equal to generation,

$$r_{CI}N_I(1 - f_0)n_0 = e_e N_I f_0, \quad (11)$$

$$r_{VI}N_I f_0 p_0 = e_h N_I(1 - f_0). \quad (12)$$

Using

$$n_0 = n_i \exp\left(\frac{E_{f0} - E_i}{kT}\right), \quad (13)$$

$$p_0 = n_i \exp\left(\frac{E_i - E_{f0}}{kT}\right), \quad (14)$$

and

$$f_0 = \frac{1}{\exp\left(\frac{E_I - E_{f0}}{kT}\right) + 1}, \quad (15)$$

where E_I is the IB energy position, we can get e_e and e_h ,

$$e_e = r_{CI} n_i \exp\left(\frac{E_I - E_i}{kT}\right), \quad (16)$$

$$e_h = r_{VI} n_i \exp\left(\frac{E_i - E_I}{kT}\right). \quad (17)$$

If there is steady light injection, electrons have a stable transition from the VB to the CB via the IB with net transition rate G_I ,

$$G_I \equiv G_{CI} - R_{CI} = G_{VI} - R_{VI}. \quad (18)$$

Solve the Eq. (18), leading to²⁰

$$f = \frac{e_h + g_{VI} + r_{CI}n}{e_e + e_h + g_{CI} + g_{VI} + r_{CI}n + r_{VI}p}, \quad (19)$$

$$G_I = \frac{N_I [e_e g_{VI} + e_h g_{CI} + g_{CI} g_{VI} - r_{CI} r_{VI} (pn - n_i^2)]}{e_e + e_h + g_{CI} + g_{VI} + r_{CI}n + r_{VI}p}. \quad (20)$$

This time if we set $g_{CI} = g_{VI} = 0$, f and G_I can be expressed as

$$f' = \frac{e_h + r_{CI}n}{e_e + e_h + r_{CI}n + r_{VI}p}, \quad (21)$$

$$G'_I = -\frac{N_I r_{CI} r_{VI} (pn - n_i^2)}{e_e + e_h + r_{CI}n + r_{VI}p}. \quad (22)$$

G_I has the form of SRH recombination, if there is no electrical injection, $n = n_0$ and $p = p_0$, so Eq. 21 becomes a equivalent expression for Eq. 15,

$$f_0 = \frac{1}{\exp\left(\frac{E_I - E_{f0}}{kT}\right) + 1} = \frac{e_h + r_{CI}n_0}{e_e + e_h + r_{CI}n_0 + r_{VI}p_0}. \quad (23)$$

The selective ohmic contact boundary conditions for Eqs. (4) and (5) are used when solving the drift-diffusion model,²³ $J_n(L) = eS_{nL}[n(L) - n_0(L)]$, $J_p(L) = -eS_{pL}[p(L) - p_0(L)]$, $J_n(R) = -eS_{nR}[n(R) - n_0(R)]$ and $J_p(R) = eS_{pR}[p(R) - p_0(R)]$, L (R) stands for left (right) boundary, S s with subscripts are surface recombination coefficients.

III. SIMULATION AND RESULTS

A. Parameters

The simulation structure is depicted in Fig. 1, the thickness of the p-region, i-region and n-region are 200, 500 and 500 nm respectively. The 50 nm QD layer is placed in the center of the i-region. The bandgap of the host material GaAs E_g is 1.424 eV, the IB energy level E_I is formed by electron ground energy level of QD, for InAs/GaAs QD $E_I = 1.124$ eV.²⁰ The solar cell is simulated under AM 1.5²³ solar spectrum with the reflectivity of the front surface $R(\lambda)$ setting to 0.1, and GaAs absorption coefficient from Ref. 24, the carrier mobilities of GaAs are related to the doping,

$$\mu_n = 1000 + \frac{7200}{1 + [(N_D + N_A)/6 \times 10^{16}]^{0.55}} \text{ cm}^2/\text{Vs}, \quad (24)$$

$$\mu_p = 32 + \frac{400}{1 + [(N_D + N_A)/1.88 \times 10^{17}]^{0.5}} \text{ cm}^2/\text{Vs}. \quad (25)$$

For r_{CI} and r_{VI} , according to Eq. 22, the lifetimes of electron and hole are $\tau'_n = 1/(N_I r_{CI})$ and $\tau'_p = 1/(N_I r_{VI})$, respectively. Due to Auger cooling effect,²⁵ electrons are no longer affected by the phonon bottleneck effect, and can easily be captured from the CB to the IB, so τ'_n is small, about 1×10^{-12} s, Auger cooling effect is beneficial to QD lasers for high modulation rate, but detrimental to QD solar cells. τ'_p is mainly determined by electron radiative recombination lifetime from the IB to the VB, $\tau'_p \approx 1 \times 10^{-9}$ s. So r_{CI} and r_{VI} are set to $1.25 \times 10^{-5} \text{ cm}^3 \text{ s}^{-1}$ and $1.25 \times 10^{-8} \text{ cm}^3 \text{ s}^{-1}$, respectively. The light generation coefficients g_{CI} and g_{VI} are from Ref. 20, which are from fitting the experimental results, $g_{CI} = g_{VI} = 2.31 \times 10^3 \text{ s}^{-1}$, to make a comparison, we also studied the case with $g_{CI} = g_{VI} = 1 \times 10^5 \text{ s}^{-1}$, which are the only parameters we assumed. Other parameters are given in Tab. I.

B. N-type doping without QDs

In order to exclude the effect of doping on the control GaAs solar cell, we first investigate the doping in the 50 nm layer without QDs. In Fig. 2, as the doping density increases from 0 to $2 \times 10^{17} \text{ cm}^{-3}$, the open circuit voltage V_{oc} increases from 0.99 to 1.01 V, while the short circuit current density J_{sc} decreases from 23.67 to 23.63 mA/cm², the fill factor from

0.82 to 0.84, and the conversion efficiency from 19.3% to 20.1%. When the doping density is 0, it is corresponding to the control GaAs solar cell and its data are noted as dashed line. The change of J_{sc} and V_{oc} are due to the change of total recombination $R_{SRH} + R_{CV}$. In Fig. 3(a), for short circuit the total recombination between the doping layer and n-region increases as the doping density increases, while the total recombination decreases when the output voltage is 1V as shown in Fig. 3(b). In fact, the doping layer has a coulomb screen effect on the region between the doping layer and the n-region, the build-in electric potential gradually falls to the region between p-region and the doping layer, and the carriers have a redistribution, so the total recombination changes accordingly.

C. Low light generation coefficients

In the calculations below, the QDs are added to the 50 nm layer. In Fig. 4, $g_{CI} = g_{VI} = 2.31 \times 10^3 \text{ s}^{-1}$, as the doping density increases from 0 to $2 \times 10^{17} \text{ cm}^{-3}$, V_{oc} increases significantly from 0.84 to 1.0 V, for the doping density larger than $1.5 \times 10^{17} \text{ cm}^{-3}$, V_{oc} is a little larger than that of the control GaAs solar cell 0.99 V. J_{sc} decreases monotonically from 23.82 to 23.65 mA/cm², for the control GaAs solar cell it is 23.67 mA/cm². The fill factor is larger than that of the control GaAs solar cell for the whole doping range, and there is a kink at doping density about $9 \times 10^{16} \text{ cm}^{-3}$, which is a little larger than N_I , it indicates the kink happens when the IB is fully occupied by electrons. What we most care the conversion efficiency increases from 17.2% to 20%, that of the control GaAs solar cell is 19.3%.

D. High light generation coefficients

To better understand the effects of the doping on current-voltage characteristic, we calculated another set of data for g_{CI} and g_{VI} , $g_{CI} = g_{VI} = 1 \times 10^5 \text{ s}^{-1}$, corresponding to high photon absorption or wide range absorption spectrum. The results are shown in Fig. 5. V_{oc} has a large increase, which is almost the same to that for low generation coefficients, while J_{sc} has a large increase with maximum value 30.07 mA/cm², it decrease to 23.66 mA/cm² as the doping density increases. The fill factor has a large fluctuation, its value is as low as 0.74 at doping density about $9 \times 10^{16} \text{ cm}^{-3}$, at which doping density there is also a kink. The conversion efficiency has a large increase compared to the result in Fig. 4(d), its maximum

value is 21.6% when there is no doping, it decreases to the smallest value 18.8% at about doping density $8 \times 10^{16} \text{cm}^{-3}$, which is equal to N_I , then increases to 20% as doping density continues to increase.

Comparing the results above, we can draw the conclusion that when the doping density is large, such as doping density greater than $1 \times 10^{17} \text{cm}^{-3}$, the increase of conversion efficiency is mainly attributed to the doping effect on the control GaAs solar cell without QDs. This is due to the IB is fully filled with electrons for the high doping density, and there are no empty states to accept electrons for transition from the VB to the IB, and the role of QDs are suppressed.

For the QD IBSC with high generation coefficients, Fig. 6(a) and Fig. 6(b) show n and p distribution in the host material GaAs for short circuit and output voltage 1 V, respectively, and the electron occupation factor f in the IB is depicted in Fig. 7. When there is no doping, f is small on short circuit condition, $-fN_I$ is small in Eq. 3, so the small amount of electrons in the IB have a little coulomb effect on n and p . When the output voltage is 1 V without doping, f is about 0.41, the electrons in the IB has a large coulomb effect, and lead to a concave in n and a convex in p as seen in Fig. 6(b). When doping density increases, under short circuit n in the region between the QD layer and n-region increases evidently, for the output voltage 1 V, n increases and p decreases at the position of the QD layer, and there is a convex in n and concave in p for large doping density.

E. Analysis and discussion

It is easy to understand the change of J_{sc} and V_{oc} as doping density increases by simply analyzing G_I . As shown in Fig. 6, n and p change as the QD layer's position, the doping density N_{dope} and output voltage V_{op} . According to Eq. 20, G_I is a function of n and p , considering the QD layer is fixed in the middle of the i-region in our study, so G_I can be written as $G_I(N_{dope}, V_{op})$.

On short circuit condition, if there is no doping, the electron and hole carrier concentration are relatively small in the middle of the i-region as shown in Fig. 6(a), so we can neglect the items about n and p in Eq. (20), therefore,

$$G_I(N_{dope} = 0, V_{op} = 0) \approx \frac{N_I(e_e g_{VI} + e_h g_{CI} + g_{CI} g_{VI})}{e_e + e_h + g_{CI} + g_{VI}}. \quad (26)$$

Because $e_e \gg e_h$, $e_e \gg g_{CI}$ and $e_e \gg g_{VI}$, $G_I(N_{dope} = 0, V_{op} = 0)$ can be further simplified, $G_I(N_{dope} = 0, V_{op} = 0) \approx N_I g_{VI}$, this means G_I is fully determined by g_{VI} on short circuit condition without doping, compared to the control GaAs solar cell its increase ΔJ_{sc} is 0.15 mA cm^{-2} in Fig. 4(b) and 6.4 mA cm^{-2} in Fig. 5(b), fully conformed to the relation

$$\Delta J_{sc} \approx e G_I w_{QD} = e N_I g_{VI} w_{QD}, \quad (27)$$

where w_{QD} is the thickness of the QD layer 50 nm. When considering the doping, n at the position of the QD layer increases, so n can not be neglect,

$$G_I(N_{dope}, V_{op} = 0) \approx \frac{N_I(e_e g_{VI} - r_{CI} r_{VI} n p)}{e_e + r_{CI} n}. \quad (28)$$

Apparently, G_I decreases monotonically as the doping density increases, so J_{sc} decreases monotonically.

On open circuit condition, according to Fig. 6(b), n and p are large, considering $e_e \gg e_h$, $e_e \gg g_{CI}$ and $e_e \gg g_{VI}$, so

$$G_I(N_{dope}, V_{op} = V_{oc}) \approx -\frac{N_I r_{CI} r_{VI} n p}{e_e + r_{CI} n + r_{VI} p}. \quad (29)$$

Due to the increase of n and $r_{CI} \gg r_{VI}$, $|G_I|$ gets smaller, that is the recombination via IB is reduced, so V_{oc} increases.

By now literatures all point out that the IB should be half-filled.^{11,14,20,26} But in our simulation model, there is no such relation between the conversion efficiency in Fig. 5(d) and its corresponding electron occupation factor in Fig. 7. With the increase of the doping, the predicted increase of light current doesn't appear in our model. Because the maximum short circuit current density is determined by Eq. 27, and can't be increased more by doping. Additionally, by comparing Eqs. 23 and 19, although the IB can be half-filled by doping, $f_0 = 0.5$, f is no long 0.5 when the solar cell works at the maximum power point.

It is noteworthy that the conversion efficiency are also affected by the fill factor, in Fig. 5 when the doping density changes from 0 to $5 \times 10^{16} \text{ cm}^{-3}$, the short circuit current density almost has no change, but the conversion efficiency decreases due to the decrease of the fill factor.

IV. CONCLUSIONS

In conclusion, the current-voltage characteristic of the IBSC is affected by the n-type doping density in the QD layer. The open circuit voltage, short current density, fill factor

and conversion efficiency all vary with the doping density. As the n-type doping density increases, the open circuit voltage increases, while the short circuit current density decreases, and the conversion efficiency tends to close to that of the control solar cell. In one word, the n-type doping tends to suppress the role of QDs, whether the QDs originally play positive or negative role. This prediction has been observed in our recent experiment, the details about growth, fabrication and experimental data will be published later.

ACKNOWLEDGMENTS

This work is supported by the National Natural Science Foundation of China (Nos.60876033, 61076050, 61021003 and 61176047) and the National Basic Research Program of China (No. 2012CB932701).

REFERENCES

- ¹A. Luque and A. Martí, Phys. Rev. Lett. **78**, 5014 (1997).
- ²A. Luque, A. Martí, and L. Cuadra, IEEE Trans. Electron Devices **48**, 2118 (2001).
- ³T. Nozawa and Y. Arakawa, Appl. Phys. Lett. **98**, 171108 (2011).
- ⁴R. B. Laghumavarapu, A. Moscho, A. Khoshakhlagh, M. El-Emawy, L. F. Lester, and D. L. Huffaker, Appl. Phys. Lett. **90**, 173125 (2007).
- ⁵V. Popescu, G. Bester, M. C. Hanna, A. G. Norman, and A. Zunger, Phys. Rev. B **78**, 205321 (2008).
- ⁶D. Guimard, R. Morihara, D. Bordel, K. Tanabe, Y. Wakayama, M. Nishioka, and Y. Arakawa, Appl. Phys. Lett. **96**, 203507 (2010).
- ⁷C. G. Bailey, D. V. Forbes, R. P. Raffaele, and S. M. Hubbard, Appl. Phys. Lett. **98**, 163105 (2011).
- ⁸N. López, L. A. Reichertz, K. M. Yu, K. Campman, and W. Walukiewicz, Phys. Rev. Lett. **106**, 028701 (2011).
- ⁹A. Luque and A. Martí, Nat. Photon. **5**, 137 (2011).
- ¹⁰S. A. Blokhin, A. V. Sakharov, A. M. Nadtochy, A. S. Pauysov, M. V. Maximov, N. N. Ledentsov, A. R. Kovsh, S. S. Mikhlin, V. M. Lantratov, S. A. Mintairov, N. A. Kaluzhniy, and M. Z. Shvarts, Semiconductors **43**, 514 (2009).
- ¹¹A. Martí, L. Cuadra, and A. Luque, IEEE Trans. Electron Devices **48**, 2394 (2001).
- ¹²A. Martí, N. López, E. Antolín, E. Cánovas, C. Stanley, C. Farmer, L. Cuadra, and A. Luque, Thin Solid Films **511512**, 638 (2006).
- ¹³A. Martí, E. Antolín, C. R. Stanley, C. D. Farmer, N. López, P. Díaz, E. Cánovas, P. G. Linares, and A. Luque, Phys. Rev. Lett. **97**, 247701 (2006).
- ¹⁴A. S. Lin, W. Wang, and J. D. Phillips, J. Appl. Phys. **105**, 064512 (2009).
- ¹⁵T. Inoue, S. Kido, K. Sasayama, T. Kita, and O. Wada, J. Appl. Phys. **108**, 063524 (2010).
- ¹⁶Y. Okada, T. Morioka, K. Yoshida, R. Oshima, Y. Shoji, T. Inoue, and T. Kita, J. Appl. Phys. **109**, 024301 (2011).
- ¹⁷T. Navruz and M. Saritas, Sol. Energy Mater. Sol. Cells **92**, 273 (2008).
- ¹⁸T. Navruz and M. Saritas, Sol. Energy Mater. Sol. Cells **93**, 1913 (2009).
- ¹⁹R. Strandberg and T. W. Reenaas, Prog. Photovoltaics Res. Appl. **19**, 21 (2011).

- ²⁰A. Luque, A. Martí, N. López, E. Antolín, E. Caínovas, C. Stanley, C. Farmer, and P. Díaz, J. Appl. Phys. **99**, 094503 (2006).
- ²¹A. Lin and J. Phillips, IEEE Trans. Electron Devices **56**, 3168 (2009).
- ²²S. M. Sze and K. K. Ng, *Physics of Semiconductor Devices* (John Wiley & Sons, 2007).
- ²³S. J. Fonash, *solar cell device physics* (Academic Press, 2010).
- ²⁴H. C. Casey, D. D. Sell, and K. W. Wecht, J. Appl. Phys. **46**, 250 (1974).
- ²⁵S. Tomicacuta, Phys. Rev. B **82**, 195321 (2010).
- ²⁶R. Strandberg and T. W. Reenaas, J. Appl. Phys. **105**, 124512 (2009).

TABLE I. Simulation parameters

Energy gap of GaAs E_g (eV)	1.424
IB energy level E_I (eV)	1.124
Permittivity ε (ε_0)	12.9
Intrinsic concentration of GaAs n_i (cm^{-3})	2.25×10^6
Density of states of the IB N_I (cm^{-3})	8×10^{16}
Donor doping density N_D (cm^{-3})	3×10^{17}
Acceptor doping density N_A (cm^{-3})	5×10^{18}
SRH electron lifetime for GaAs τ_n (s)	2×10^{-9}
SRH hole lifetime for GaAs τ_p (s)	4×10^{-7}
CB to IB recombination coefficient r_{CI} ($\text{cm}^3 \text{s}^{-1}$)	1.25×10^{-5}
IB to VB recombination coefficient r_{VI} ($\text{cm}^3 \text{s}^{-1}$)	1.25×10^{-8}
Surface recombination coefficient s_{nL}, s_{pR} (cm s^{-1})	1×10^4
Surface recombination coefficient s_{nR}, s_{pL} (cm s^{-1})	1×10^7
CB to VB direct recombination coefficient r_{CV} ($\text{cm}^3 \text{s}^{-1}$)	7.2×10^{-10}

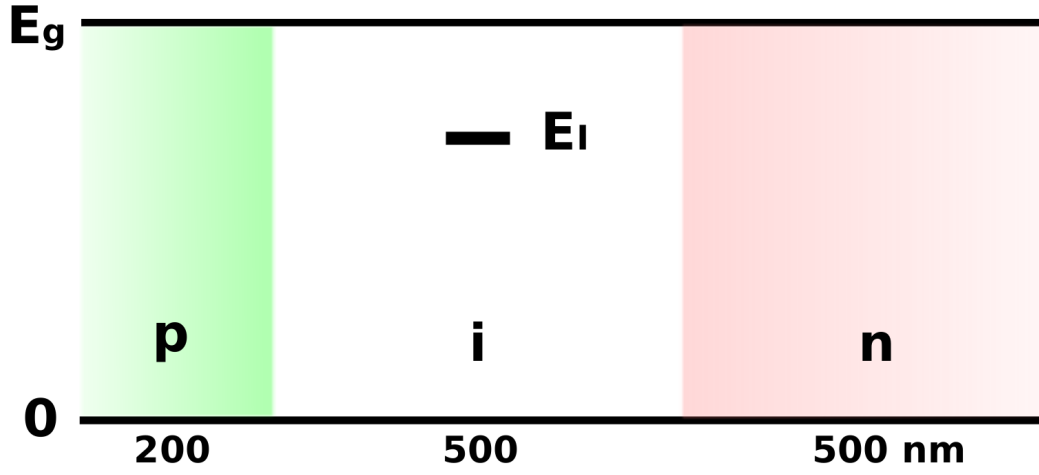


FIG. 1. (Color online) The simulation structure, the 50 nm QD layer is placed in the middle of the i-region.

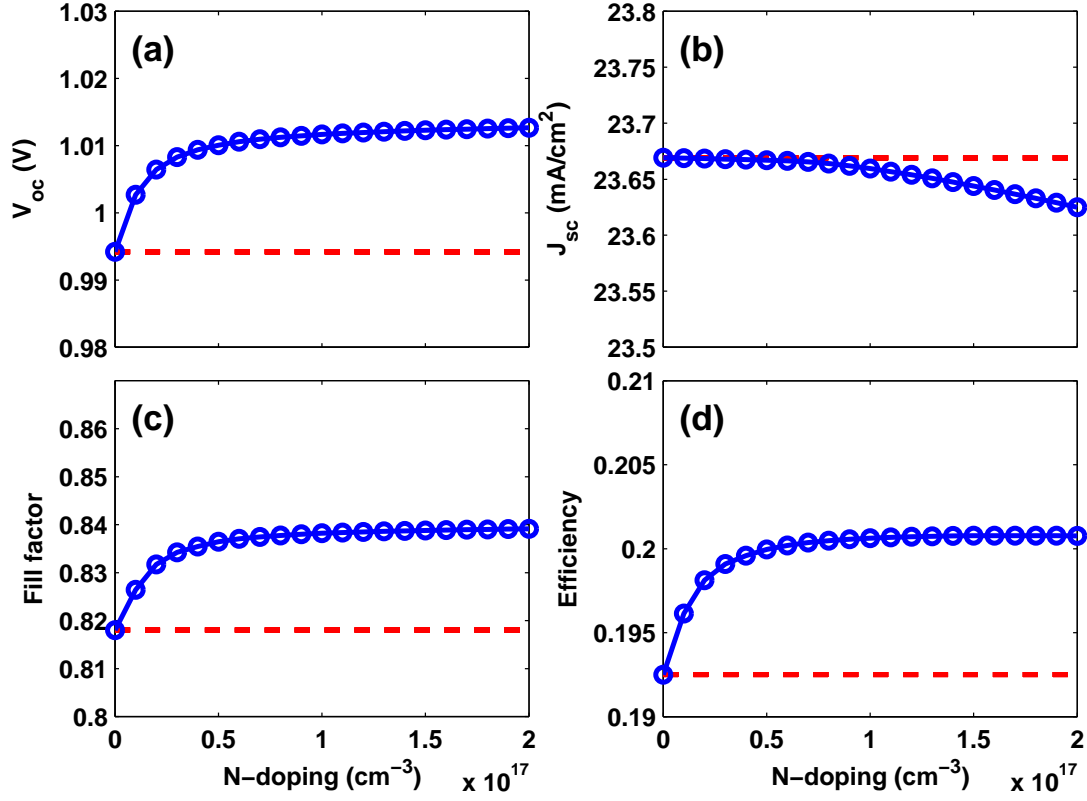


FIG. 2. (Color online) Doping without QDs, the current-voltage characteristic changes as the doping density increases. (a) Open circuit voltage. (b) Short circuit current density. (c) Fill factor. (d) Conversion efficiency. Data for the control GaAs solar cell without QD layer are plotted as dashed lines.

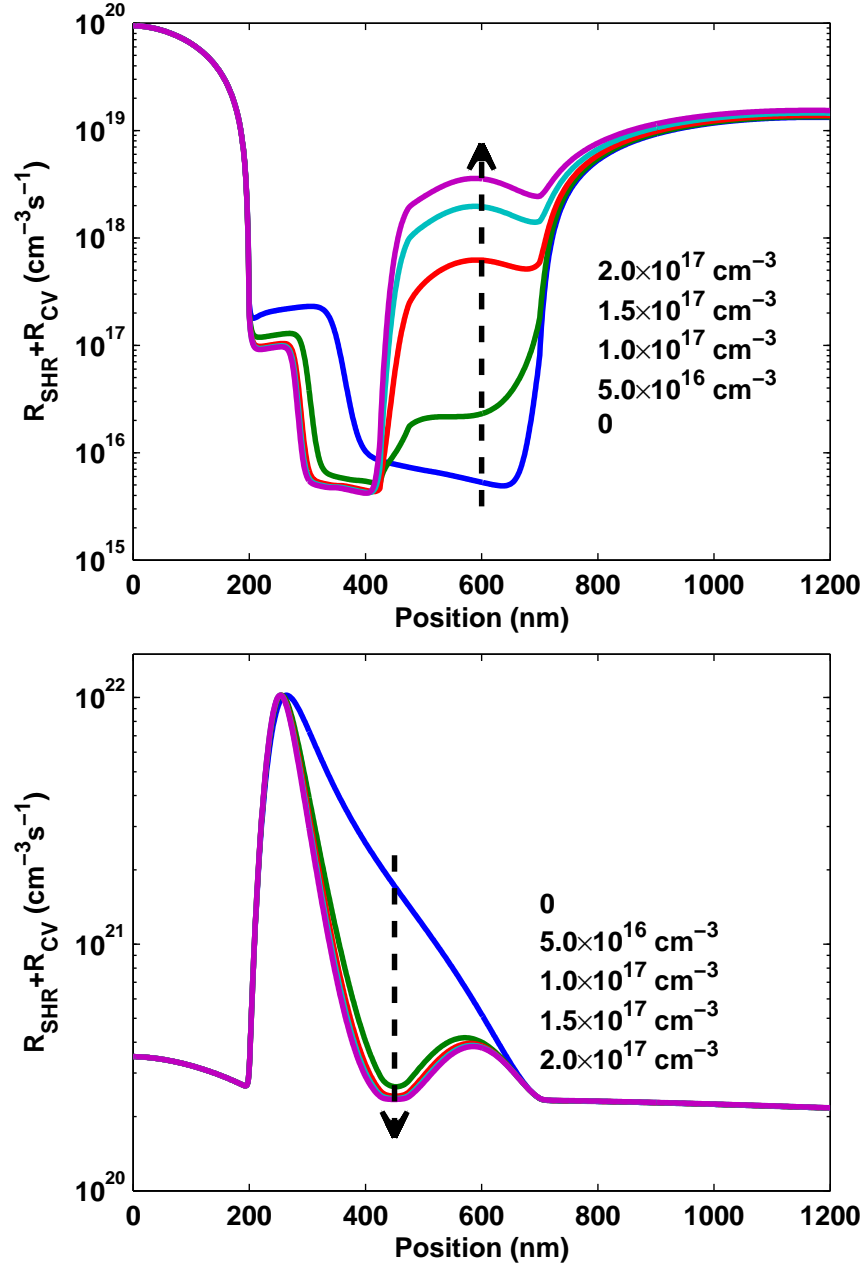


FIG. 3. (Color online) Doping without QDs, the total recombination $R_{SRH} + R_{CV}$ changes as different doping density. (a) On short circuit condition. (b) When the output voltage is 1 V. Data for the control GaAs solar cell without QD layer and doping are plotted as dashed line.

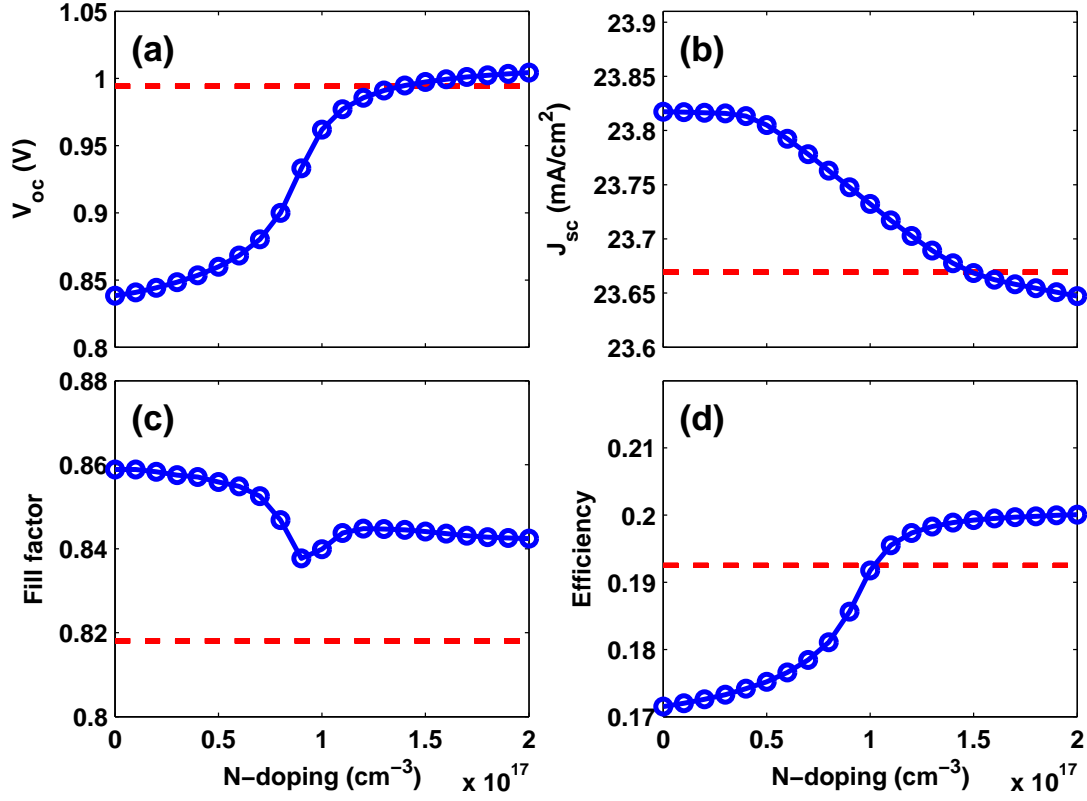


FIG. 4. (Color online) For $g_{CI} = g_{VI} = 2.31 \times 10^3 \text{ s}^{-1}$, the current-voltage characteristic changes as the doping density increases. (a) Open circuit voltage. (b) Short circuit current density. (c) Fill factor. (d) Conversion efficiency. Data for the control GaAs solar cell without QD layer are plotted as dashed lines.

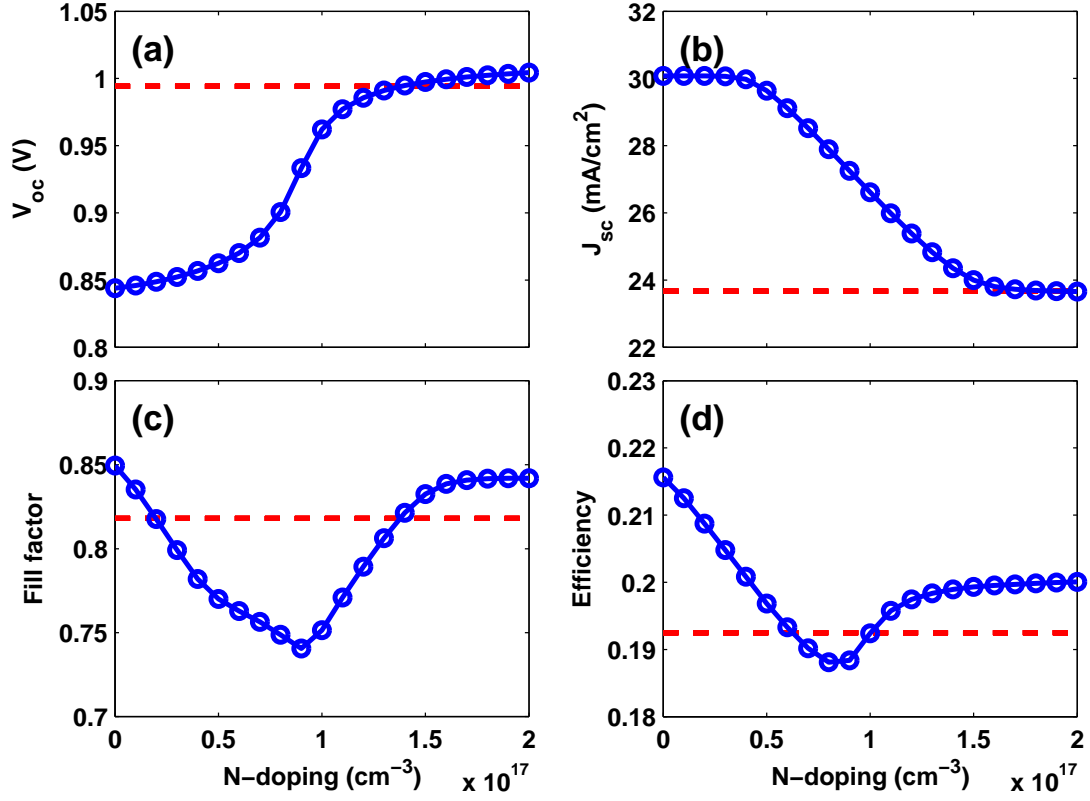


FIG. 5. (Color online) For $g_{CI} = g_{VI} = 1 \times 10^5 \text{ s}^{-1}$, the current-voltage characteristic changes as the doping density increases. (a) Open circuit voltage. (b) Short circuit current density. (c) Fill factor. (d) Conversion efficiency. Data for the control GaAs solar cell without QD layer are plotted as dashed lines.

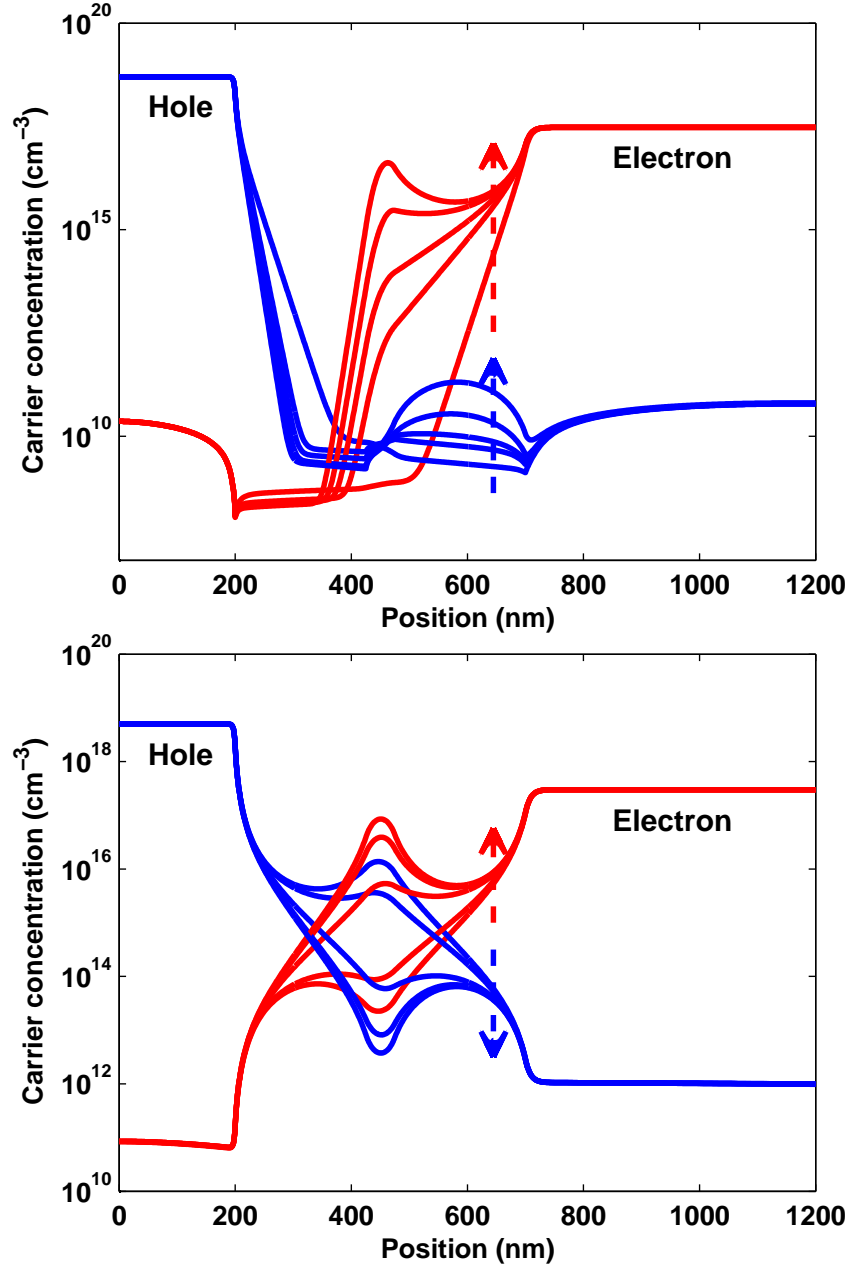


FIG. 6. (Color online) For $g_{CI} = g_{VI} = 1 \times 10^5 \text{ s}^{-1}$, the carrier concentration of electron and hole in the GaAs host material for the doping density $0, 5 \times 10^{16}, 1 \times 10^{17}, 1.5 \times 10^{17}$ and $2 \times 10^{17} \text{ cm}^{-3}$. (a) On short circuit condition (b) When output voltage is 1 V. The dashed arrow indicates the change direction as doping density increases.

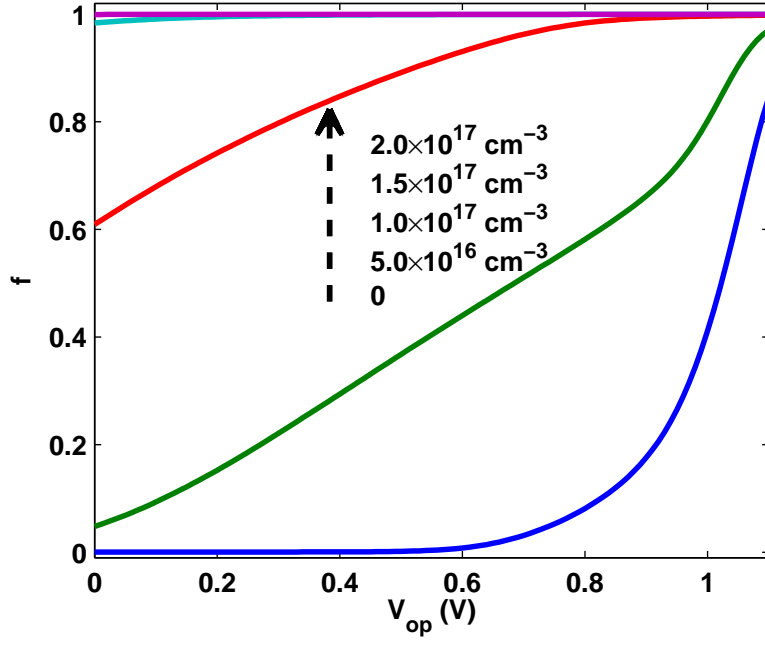


FIG. 7. (Color online) For $g_{CI} = g_{VI} = 1 \times 10^5 \text{ s}^{-1}$, the electron occupation factor f in the IB vs. output voltage V_{op} with different doping density. The dashed arrow indicates the change direction as doping density increases.